Prepared for submission to JHEP

Some aspects of QGP phase in a hQCD model

Rong-Gen Cai[a] **Shankhadeep Chakrabortty,**[b] **Song He,**[a] **Li Li,**[a]

[a] *State Key Laboratory of Theoretical Physics, Institute of Theoretical Physics, Chinese Academy of Science, Beijing 100190, People's Republic of China*

[b] *Institute of Physics, Bhubaneswar 751 005, India*

E-mail: cairg@itp.ac.cn, sankha@iopb.res.in, hesong@itp.ac.cn, liliphy@itp.ac.cn

Abstract: We continue to study the holographic QCD (hQCD) model, proposed in a previous paper, in an Einstein-Maxwell-Dilaton (EMD) system. In this paper we discuss some aspects of quark gluon plasma (QGP) in the hQCD model, such as drag force, jet quenching parameter and screening length. The results turn out to be consistent with those as expected in QCD qualitatively. By calculating free energy of the background black hole solution, we find that there exists a phase transition between small black hole and large black hole when chemical potential μ is less than the critical one μ_c, and the phase transition is absent when chemical potential is beyond the critical one.

Keywords: Einstein-Maxwell-Dilaton system, black hole solution, quark gluon plasma, AdS/CFT

Contents

1 Introduction

The analysis of various dynamical quantities from the experimental data obtained at Relativistic Heavy Ion Collider (RHIC) in Brookhaven National Laboratory leads to strong evidence for a strong coupled quark gluon plasma (QGP), a deconfined phase of QCD at high temperature and high number density [1], [2], [3]. In the Au+Au collision with the maximum center-of-mass energy around 200 GeV, several phenomenological features, e.g, a very small value of shear viscosity, quenching of high energy partons with large transverse momentum, and elliptic flow etc., indicate that the dynamics of thermal medium produced after collision is dominated by non-perturbative effects [4]. Being formulated in Euclidean time, lattice QCD seems to be the best candidate to explain the phenomena in thermal equilibrium, while the perturbative QCD works only in the weak coupling region. But, both the perturbative QCD and lattice QCD are failed to compute some dynamical quantities like transport coefficients, drag force, and jet quenching parameter etc., in the strong coupling regime. Thanks to the feature of strong/weak coupling duality, the AdS/CFT correspondence [5] [6] provides a powerful tool to stress those issues.

In the AdS/CFT correspondence, a well-known example of strong/weak duality is AdS_5/CFT_4 and in this case, the four dimensional conformal field theory is $\mathcal{N} = 4$ $SU(N_c)$ super Yang-Mills (SYM), while the bulk theory is the type IIB supergravity in AdS_5. In the AdS_5/CFT_4 correspondence, the ratio of shear viscosity over entropy density for the dual field theory is found to be small ($\eta/s = 1/4\pi$) for large number of colors (N_C) and

large 't Hooft coupling ($\lambda = {g_{YM}}^2 N_C$) [7] [8] [9]. It turns out that this value is consistent with the one from RHIC data with experimental error [10]. In addition, it is found that the value $1/4\pi$ is universal for various deformations of the gauge theories with gravity duals. Another example of the universality is discussed in [11], where it is found that for some gauge theories (not necessarily conformal) with well defined gravity duals where if some conditions on the bulk stress energy tensor are satisfied, the electrical conductivity at finite chemical potential (μ) and temperature (T), the thermal conductivity (κ_T) and the ratio of thermal conductivity to viscosity ($\frac{\kappa_T}{\eta T}\mu^2$) are independent of any specific model.

Certainly a realistic holographic model dual to the strong coupled QCD at finite temperature and finite density is a good starting point to study the RHIC physics. Unfortunately such a model is still absent. However, due to the universality mentioned above, one is expecting to understand various features of QGP at RHIC with some deformed AdS_5/CFT_4, such as drag force, jet-quenching parameter, and screening-length etc. Indeed, over the past years a lot of works have been done along this line.

By employing the so-called potential reconstruction approach [12–15] to build up holographic QCD model [16] from bottom up point of view, a hQCD model in an Einstein-Maxwell-dilaton theory is proposed in [15]. In [14, 15], some properties of the hQCD model are studied, such as equation of state, Wilson line operators [12] and confinement/deconfinement phase transition and associated phase diagram [15], with good agreement with lattice QCD simulation. It shows that this model can capture some most important characteristics of realistic QCD. In this paper, we continue to study the hQCD model by investigating some aspects of QGP phase such as drag force, jet quenching parameter as well as screening length. The results show that these quantities are consistent with QGP properties. In this sense, we further confirm that this model may give us the hints on the efficient way to deform the pure AdS_5 geometry and to realize the holographic description of low energy QCD.

When high-energy partons perform a dragged motion as they pass through the QGP medium, their energy loss can be encoded by drag force. In the AdS/CFT correspondence, an external heavy quark and its gluonic neighborhood are mapped into the endpoint of fundamental string attached to the AdS boundary and the string itself in the AdS bulk geometry, respectively. This external quark, with mass proportional to the length of the string, loses its energy as the string trailing back imposes a drag force on it. Within the framework of gauge/gravity duality, the drag force experienced by an external heavy quark moving with a constant velocity in $\mathcal{N} = 4$ super Yang-Mills plasma at finite temperature is computed [17], [18], [19], [20], [21], [22], [23]. There are also further generalizations of drag force computation for the charged $\mathcal{N} = 4$ SYM [24] and with the backreaction effect due to the static heavy quark cloud distribution [25].

Due to the medium, the suppression of heavy quark with high transverse momentum leads to energy loss which is so called jet quenching phenomenon [26], [27], [28]. The transport coefficient $\hat{q}$ [29], characterizing such phenomena, is defined perturbatively as the ratio of square of the mean transverse momentum over the mean free path [30]. With the framework of eikonal approximation [31], [32], the parameter $\hat{q}$ can be calculated from light-like Wilson loop in adjoint representation [33], [34], [35], [36], [37], [38], [39]. Ref. [40]

and [41] calculate the jet quenching parameter in the presence of chemical potential. Using AdS/CFT, the quark-antiquark pair is mapped to the two endpoints of a fundamental string, both endpoints attach on the AdS boundary. The string configuration shows it hangs down to the bulk along radial direction and turns back to the boundary again. The light-like Wilson loop in the fundamental representation of boundary gauge theory and its thermal expectation value correspond to the trajectory of two endpoints of the string and $\exp(S)$ respectively, where S is the string Nambu-Goto action. In addition, we further extend our analysis by studying the time-like Wilson loop and relate it with another important parameter, the screening length of a quark-antiquark pair. It is defined as the maximum length between a moving $q\bar{q}$ pair, beyond which they break off with no binding energy and thus become screened in the QGP medium. Screening length depends on the velocity and the orientation of the quark-antiquark pair with respect to the medium. Treating $\mathcal{N} = 4$ SYM at finite temperature as a boundary theory, the binding energy between quark and antiquark pair moving in the QGP and the screening length are calculated in [42]. There are also other important generalizations to calculate these quantities by introducing a boost on the original static background [43], [44], [45]. In this paper we will calculate the screening length in the static frame of $q\bar{q}$ pair for our hQCD model.

In [15] we calculated heavy quark potential between a quark-antiquark pair in our model, and found that there is a confinement/deconfinement phase transition, and that there is a critical point in the $T - \mu$ phase diagram. In this paper we further confirm this phase transition in the small μ region by computing free energy of the background black hole solution by using the method in [46]. In the AdS/CFT correspondence, the Hawking-Page phase transition [47] between AdS black hole and thermal gas in AdS space is identified with the confinement/deconfiement transition in gauge theory [48][49][50][51]. In our case, the phase transition happens between small black hole and large black hole, which will be clear shortly. In addition, we will argue that there is no phase transition between black hole solution and thermal gas solution in our model.

The organization of the paper is as follows. In section 2 we briefly review the potential reconstruction approach to the Einstein-Maxwell-Dilaton system by generalizing the discussion in [15] to the case with a coupling between dilaton field and Maxwell field. In section 3, we discuss the generic black hole solutions with asymptotical AdS boundary, and in particular present an analytic black hole solution. In addition, in this section we also briefly review the black hole solution for the hQCD model studied in [15]. In section 4, we calculate the drag force in this hQCD model. The jet quenching parameter and screening length are discussed in section 5 and 6, respectively. In section 7, we study the free energy of the background black hole solution and discuss the phase transition between small black hole and large black hole in small chemical potential region. Section 8 is devoted to conclusions and discussions.

2 Einstein-Maxwell-Dilaton system

In this section, we use the potential reconstruction approach [12, 15] to study a 5D Einstein-Maxwell-Dilaton (EMD) system. In [15], the authors did not consider the coupling between

gauge field and dilaton field in Einstein frame. Here we take the coupling into consideration in a more generic version

$$S_{5D}=\frac{1}{16\pi G_5}\int d^5x\sqrt{-g^S}e^{-2\phi}\left(R^S+4\partial_\mu\phi\partial^\mu\phi-V_S(\phi)-\frac{Z(\phi)}{4g_g^2}e^{\frac{-4\phi}{3}}F_{\mu\nu}F^{\mu\nu}\right), \quad (2.1)$$

where the action (2.1) is written in string frame, $F_{\mu\nu}=\partial_\mu A_\nu-\partial_\nu A_\mu$ is the Maxwell field, $Z(\phi)$ is an arbitrary function of dilaton field ϕ and $V_S(\phi)$ is the dilaton potential. In Einstein frame we can rewrite the action as [12]

$$S_{5D}=\frac{1}{16\pi G_5}\int d^5x\sqrt{-g^E}\left(R-\frac{4}{3}\partial_\mu\phi\partial^\mu\phi-V_E(\phi)-\frac{Z(\phi)}{4g_g^2}F_{\mu\nu}F^{\mu\nu}\right), \quad (2.2)$$

where $V_S=V_E e^{\frac{-4\phi}{3}}$. The metrics in these two frames are connected by the scaling transformation

$$g^S_{\mu\nu}=e^{\frac{4\phi}{3}}g^E_{\mu\nu}. \quad (2.3)$$

The Einstein equations from the action (2.2) read

$$E_{\mu\nu}+\frac{1}{2}g^E_{\mu\nu}\left(\frac{4}{3}\partial_\mu\phi\partial^\mu\phi+V_E(\phi)\right)-\frac{4}{3}\partial_\mu\phi\partial_\nu\phi-\frac{Z(\phi)}{2g_g^2}\left(F_{\mu k}F_\nu{}^k-\frac{1}{4}g^E_{\mu\nu}F_{kl}F^{kl}\right)=0 \quad (2.4)$$

where $E_{\mu\nu}=R_{\mu\nu}-\frac{1}{2}Rg_{\mu\nu}$ is Einstein tensor. We here consider the ansatz $A=A_0(z)dt,\quad \phi=\phi(z)$ for matter fields and

$$ds^2_S=\frac{\ell^2e^{2A_s}}{z^2}\left(-f(z)dt^2+\frac{dz^2}{f(z)}+dx^idx^i\right), \quad (2.5)$$

for the metric in string frame, where $i=1,2,3$, ℓ is the radius of AdS_5 space, and A_s is the warped factor, a function of coordinate z. The metric in the string frame will be used to calculate the loop operator below. In Einstein frame the metric reads

$$\begin{aligned}ds^2_E&=\frac{\ell^2e^{2A_e}}{z^2}\left(-f(z)dt^2+\frac{dz^2}{f(z)}+dx^idx^i\right),\\&=\frac{\ell^2e^{2A_s-\frac{4\phi}{3}}}{z^2}\left(-f(z)dt^2+\frac{dz^2}{f(z)}+dx^idx^i\right),\end{aligned} \quad (2.6)$$

with $A_e=A_s-2\phi/3$. In the metric (2.6), the $(t,t),(z,z)$ and (x_i,x_i) components of Einstein equations are respectively

$$\begin{aligned}&b''(z)+\frac{b'(z)f'(z)}{2f(z)}-\frac{b'(z)^2}{2b(z)}+\frac{4}{9}b(z)\phi'(z)^2+\frac{A_0{}'(z)^2Z(\phi)}{6g_g^2f(z)}+\frac{V_E(\phi)b(z)^2}{3f(z)}=0,\\&\phi'(z)^2-\frac{9b'(z)f'(z)}{8b(z)f(z)}-\frac{9b'(z)^2}{4b(z)^2}-\frac{3A_0{}'(z)^2Z(\phi)}{8g_g^2b(z)f(z)}-\frac{3V_E(\phi)b(z)}{4f(z)}=0,\\&f''(z)+\frac{3b'(z)f'(z)}{b(z)}+\frac{4}{3}f(z)\phi'(z)^2+\frac{3f(z)b''(z)}{b(z)}-\frac{3f(z)b'(z)^2}{2b(z)^2}-\frac{A_0{}'(z)^2Z(\phi)}{2g_g^2b(z)}+V_E(\phi)b(z)=0,\end{aligned} \quad (2.7)$$

where $b(z) = \ell^2 e^{2A_e}/z^2$, and $A_0(z)$ is electrical potential of Maxwell field. From those three equations one can obtain following two equations which do not contain the dilaton potential $V_E(\phi)$,

$$A_s''(z) + A_s'(z)\left(\frac{4\phi'(z)}{3} + \frac{2}{z}\right) - A_s'(z)^2 - \frac{2\phi''(z)}{3} - \frac{4\phi'(z)}{3z} = 0, \tag{2.8}$$

$$f''(z) + f'(z)\left(3A_s'(z) - 2\phi'(z) - \frac{3}{z}\right) - \frac{z^2 Z(\phi) e^{\frac{4\phi(z)}{3} - 2A_s(z)} A_0'(z)^2}{g_g^2 L^2} = 0. \tag{2.9}$$

Eq.(2.8) is our starting point to find exact solutions of the system. Note that Eq.(2.8) in the EMD system is the same as the one in the Einstein-dilaton system considered in [13][14] and the last term in Eq.(2.9) is an additional contribution from electrical field. In addition, the equation of motion (EOM) of the dilaton field is given by

$$\frac{8}{3}\partial_z\left(\frac{\ell^3 e^{3A_s(z)-2\phi} f(z)}{z^3}\partial_z\phi\right) - \frac{\ell^5 e^{5A_s(z)-\frac{10}{3}\phi}}{z^5}\partial_\phi V_E(\phi) + \frac{Z'(\phi) b(z) A_0'(z)^2}{2g_g^2} = 0. \tag{2.10}$$

And the EOM of the Maxwell field is given by

$$\frac{1}{\sqrt{-g^E}}\partial_\mu\left(\sqrt{-g^E} Z(\phi) F^{\mu\nu}\right) = 0. \tag{2.11}$$

From equations of motion, once $A_s(z)$ is given, we can obtain a general solution to the system, which takes the following form

$$\phi(z) = \int_0^z \frac{e^{2A_s(x)}\left(\frac{3}{2}\int_0^x y^2 e^{-2A_s(y)} A_s'(y)^2\, dy + \phi_1\right)}{x^2}\, dx + \frac{3A_s(z)}{2} + \phi_0, \tag{2.12}$$

$$A_0(z) = A_{00} + A_{01}\left(\int_0^z \frac{y e^{\frac{2\phi(y)}{3} - A_s(y)}}{Z(\phi(y))}\, dy\right), \tag{2.13}$$

$$f(z) = \int_0^z x^3 e^{2\phi(x)-3A_s(x)}\left(\frac{{A_{01}}^2\left(\int_0^x \frac{y e^{\frac{2\phi(y)}{3} - A_s(y)}}{Z(\phi(y))}\, dy\right)}{g_g^2\ell^2} + f_1\right) dx + f_0, \tag{2.14}$$

$$\begin{aligned} V_E(z) = {} & \frac{e^{-2A_s(z)+\frac{4\phi(z)}{3}} z^2 f(z)}{\ell^2} 2\Big(- \frac{e^{-2A_s(z)+\frac{4\phi(z)}{3}} Z(\phi(z)) z^2 A_0'(z)^2}{4g_g^2\ell^2 f(z)} \\ & - \frac{2\left(3 + 3z^2 A_s'(z)^2 + 4z\phi'(z) + z^2\phi'(z)^2 - 2zA_s'(z)\left(3 + 2z\phi'(z)\right)\right)}{z^2} \\ & - \frac{f'(z)\left(-3 + 3zA_s'(z) - 2z\phi'(z)\right)}{2zf(z)}\Big), \end{aligned} \tag{2.15}$$

where $\phi_0, A_{00}, A_{01}, f_0, f_1$ are all integration constants and can be determined by suitable UV and IR boundary conditions. When $Z(\phi) = 1$, the general solution reduces to the one given in [15]. Thus we have given a generic formulism to generate a set of exact solutions of the EMD system with a given $A_s(z)$.

3 General asymptotical AdS black hole solutions

Since here we are only interested in the black hole solutions with asymptotic AdS boundary, we impose the boundary condition $f(0) = 1$ at the AdS boundary $z = 0$, and require $\phi(z), f(z), A_0(z)$ to be regular at black hole horizon z_h and AdS boundary $z = 0$. There is an additional condition $A_0(z_h) = 0$, which corresponds to the physical requirement that $A_\mu A^\mu = g^{tt} A_0 A_0$ must be finite at $z = z_h$.

We can parameterize the function $f(z)$ in Eq.(2.12) as

$$f(z) = 1 + \frac{A_{01}^2}{2g_g^2\ell^2} \frac{\int_0^z g(x) \left(\int_0^{z_h} g(r)dr \int_r^x \frac{g(y)^{\frac{1}{3}} dy}{Z(\phi(y))} \right) dx}{\int_0^{z_h} g(x)dx} - \frac{\int_0^z g(x)dx}{\int_0^{z_h} g(x)dx}, \tag{3.1}$$

where $f_0 = 1$, $f_1 = -\frac{A_{01}^2}{4g_g^2\ell^2} \frac{\int_0^{z_h} g(x) \int_0^x \frac{g(y)^{\frac{1}{3}}}{Z(\phi(y))} dy + 1}{\int_0^{z_h} g(x)dx}$ and

$$g(x) = x^3 e^{2\phi(x) - 3A_s(x)}. \tag{3.2}$$

We expand the gauge field near the AdS boundary to relate the two integration constants to chemical potential and charge density, respectively,

$$A_0(z) \sim A_{00} + A_{01} \frac{e^{\frac{2\phi(y)}{3} - A_s(y)}}{Z(\phi(y))} z^2 + \cdots, \tag{3.3}$$

with

$$A_{00} = \mu, \tag{3.4}$$

$$A_{01} = \frac{\mu}{\int_0^{z_h} y \frac{e^{\frac{2\phi}{3} - A_s(y)}}{Z(\phi(y))} dy} = \frac{\mu}{\int_0^{z_h} \frac{g(y)^{\frac{1}{3}}}{Z(\phi(y))} dy}. \tag{3.5}$$

The temperature of the black hole can be determined through the function $f(z)$ in (3.1) as

$$T = \frac{1}{4\pi} |f'(z)|_{z=z_h} = \left| \frac{A_{01}^2}{4\pi g_g^2 \ell^2} \frac{g(z_h) \int_0^{z_h} g(r)dr \int_r^{z_h} \frac{g^{\frac{1}{3}}(y)}{Z(\phi(y))} dy - g(z_h)}{\int_0^{z_h} g(x)dx} \right|. \tag{3.6}$$

Following the standard Bekenstein-Hawking entropy formula, from the geometry given in Eq.(2.6), we obtain the black hole entropy density S as

$$S = \frac{A_{area}}{4G_5 V_3} = \frac{\ell^3}{4G_5} \left(\frac{e^{A_s - \frac{2}{3}\phi}}{z} \right)^3 \Big|_{z_h}, \tag{3.7}$$

where V_3 is the volume of the black hole spatial directions spanned by coordinates x_i in (2.6).

3.1 An analytical black hole solution

In this subsection, we list an analytical solution of the Einstein-Maxwell-Dilaton system by using Eq.(2.12-2.15) with $Z(\phi) = 1$. We impose the constrain $f(0) = 1$, and require $\phi(z), f(z)$ to be regular at $z = 0$, and z_h. We give the solution in Einstein frame as

$$ds_E^2 = \frac{\ell^2 e^{2A_e}}{z^2}\left(-f(z)dt^2 + \frac{dz^2}{f(z)} + dx^i dx^i\right), \tag{3.8}$$

with

$$\begin{aligned}
A_e(z) &= \log\left(\frac{z}{z_0\sinh(\frac{z}{z_0})}\right),\\
f(z) &= 1 - \frac{4V_{11}}{3}(3\sinh^4(\frac{z}{z_0}) + 2\sinh^6(\frac{z}{z_0})) + \frac{1}{8}V_{12}^2\sinh^4\left(\frac{z}{z_0}\right),\\
\phi(z) &= \frac{3z}{2z_0},\\
A_0(z) &= \mu - \frac{2g_g\ell}{z_0}V_{12}\sinh^2\left(\frac{z}{2z_0}\right),
\end{aligned} \tag{3.9}$$

where z_0 is an integration constant and V_{11}, V_{12} are two constants from the dilaton potential

$$V_E(\phi) = -\frac{12 + 9\sinh^2\left(\frac{2\phi}{3}\right) + 16V_{11}\sinh^6\left(\frac{\phi}{3}\right)}{\ell^2} + \frac{V_{12}^2\sinh^6\left(\frac{2\phi}{3}\right)}{8\ell^2}. \tag{3.10}$$

The two integration constants V_{11} and V_{12} then can be expressed in terms of horizon z_h and chemical potential μ as

$$\begin{aligned}
V_{11} &= \frac{3\cosh^4\left(\frac{z_h}{2z_0}\right)\left(\frac{\mu^2 z_0^2\sinh^4\left(\frac{z_h}{z_0}\right)\cosh^4\left(\frac{z_h}{2z_0}\right)}{4g_g^2\ell^2} + 8\right)}{32\left(2\sinh^2\left(\frac{z_h}{2z_0}\right) + 3\right)},\\
V_{12} &= \frac{\mu z_0\cosh^2\left(\frac{z_h}{2z_0}\right)}{2g_g\ell}.
\end{aligned} \tag{3.11}$$

We can obtain the temperature of the black hole by using Eq.(3.6) based on the above formulas. In Figure [1], we show the temperature as a function of horizon radius z_h in cases of three different chemical potentials μ. In this plot we take parameters $\ell = 1, z_0 = 1, g_g = 1$. We see from Figure [1] that the temperature with respect to horizon z_h is monotonic for a fixed chemical potential. A vanishing temperature means that the black hole is extremal with a smallest horizon radius. The smallest horizon radius increases as chemical potential becomes large.

3.2 The hQCD model

Based on the general solutions, in Ref. [15], a holographic QCD model is proposed to realize the confinement/deconfinement phase transition of QCD. Since the aim of this paper is to

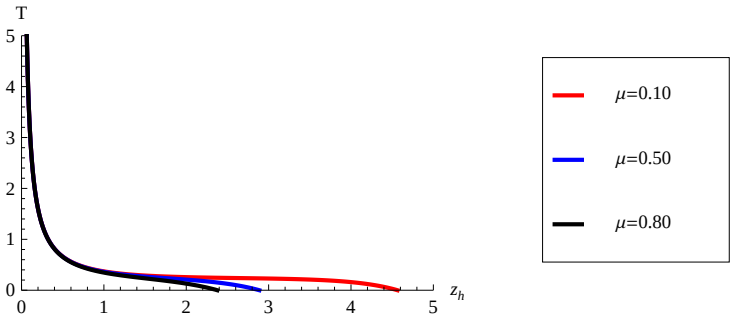

Figure 1. The temperature as a function of horizon radius z_h for the analytical black hole solution with parameters $\ell = 1, z_0 = 1, g_g = 1$.

further study the hQCD model, we here briefly review the main features of the model. In our hQCD model, the warped factor $A_s(z)$ takes the form

$$A_s(z) = k^2 z^2, \tag{3.12}$$

where k is a constant. To take this factor has various phenomenological motivations in order to build a successful holographic QCD model, for details see [15]. In this paper, we set $k = 0.3\text{GeV}$, following Ref. [15]. With this factor, we have the dilaton field ϕ as

$$\phi(z) = \frac{3}{4} k^2 z^2 (1 + H(z)), \tag{3.13}$$

where we have set the integration constant $\phi_0 = 0$, and $H(z)$ is given by

$$H(z) = {}_2F_2\left(1, 1; 2, \frac{5}{2}; 2k^2 z^2\right). \tag{3.14}$$

The characteristic function of the black hole background takes the form

$$\begin{aligned} f(z) = \; & 1 + \frac{1}{4 g_g^2 \ell^2} \left(\frac{\mu}{\int_0^{z_h} g(y)^{\frac{1}{3}} dy} \right)^2 \frac{\int_0^z g(x) \left(\int_0^{z_h} g(r) dr \int_r^x g(y)^{\frac{1}{3}} dy \right) dx}{\int_0^{z_h} g(x) dx} \\ & - \frac{\int_0^z g(x) dx}{\int_0^{z_h} g(x) dx}, \end{aligned} \tag{3.15}$$

where

$$g(x) = x^3 e^{\frac{3}{2} k^2 x^2 (1 + H(x)) - 3 k^2 x^2}. \tag{3.16}$$

One can clearly see that the second term in (3.15) comes from the contribution of electric field. If one turns off the electric field, one can reproduce the black hole solution in Einstein-dilaton system [13]. In addition, the electric field $A_t(z)$ is given by

$$A_t(z) = \mu + \frac{\mu}{\int_0^{z_h} g(y)^{\frac{1}{3}} dy} \int_0^z x e^{\frac{1}{2} k^2 x^2 (-1 + H(x))} dx. \tag{3.17}$$

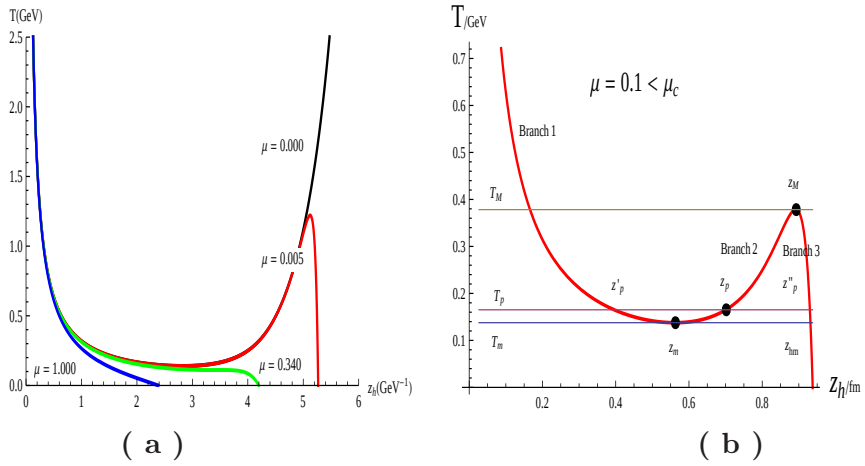

Figure 2. Plot (a): The black hole temperature as a function of horizon z_h with different chemical potentials. When $\mu > \mu_c$ the temperature monotonically decreases to zero with increase of z_h; when $0 < \mu < \mu_c$, the temperature decreases to a minimum at z_m and grows up to a maximum at z_M and then decreases to zero monotonically. When $\mu = \mu_c$, one has $z_m = z_M$. Plot (b): The temperature of the black hole with $\mu = 0.1$GeV. The three black hole solutions with horizon z'_p, z_p and z''_p have the same temperature. The black hole with $z_m < z_p < z_M$ is thermodynamically unstable. Here we take $g_g\ell = 1, k = 0.3$GeV. In this hQCD model, we always fix $k = 0.3$GeV and accordingly the critical chemical potential is $\mu_c = 0.34$GeV, which corresponds to the case $z_m = z_M$.

The temperature behavior of the black hole solution is discussed in some details in [15], with respect to horizon radius and chemical potential. To be complete and for later use, we here briefly repeat some main salient features. In Figure [2] we plot the temperature with respect to horizon radius z_h with different chemical potentials. One can see clearly that the temperature behavior crucially depends on the value of chemical potential: there is a critical chemical potential μ_c, beyond which the black hole is always thermodynamically stable, while when the chemical potential is less than the critical one, there is a region of horizon radius, where the black hole is thermodynamically unstable with negative heat capacity. To be more clear we plot in Figure [2](b) the temperature versus the horizon z_h in the case $\mu = 0.1\text{GeV} < \mu_c$ as an example. One can see from the figure that the black hole is thermodynamically unstable in the region $z_m < z_h < z_M$ (branch 2 in plot b), where z_m and z_M are the black hole horizons corresponding to the minimal and maximal temperatures (T_m and T_M), respectively. In this region, the heat capacity of the black hole is negative. The black hole solutions in the regions $z_h < z_m$ and $z_h > z_M$ are thermodynamically stable (branch 1 and branch 3). When $\mu \geq \mu_c$, z_m and z_M are degenerated to one point. Note that in contrast to the case in Figure [1], there are local minimal and maximal values of temperature in small μ cases. This is crucial to realize the critical point in the $T - \mu$ phase diagram of the hQCD model [15].

At this stage let us mention that it is quite interesting to compare the temperature behavior of our black hole solution (see Figure [2]) with the one for the Reissner-Nordström-AdS black hole (see Figure 3 of Ref. [52]). They look quite similar. But there exist

essentially different points between them. At first, in our case, the temperature is plotted with respect to horizon radius z_h for a fixed chemical potential, while in [52] it is plotted with respect to horizon radius for a fixed charge (note that there the horizon radius r_+ corresponds to the inverse of horizon radius z_h here). Second, our black hole solution has a Ricci flat horizon, while the black hole horizon discussed in [52] is a sphere. The third is that we will discuss the phase transition in grand canonical ensemble (for a fixed chemical potential) while the phase transition between a small black hole and a large black hole discussed in [52] is in canonical ensemble (for a fixed charge). As we will see shortly that just due to the similarity of temperature behavior, in our case, the phase transition will also appear between a small black hole and a large black hole in grand canonical ensemble when the chemical potential is less than the critical value.

4 Drag force

In this section, mainly following [18] we compute the drag force experienced by an external probe quark traversing in the QGP in the present hQCD model. The holographic computation of the drag force is based on the gauge/gravity correspondence between the deconfined phase of hQCD model at finite temperature and its dual garvity realized as an aAdS black hole solution in the Einstein-Maxwell-Dilaton background. In this aAdS black hole geometry, the gravity dual of the probe quark is described by an infinitely long fundamental string. One of its ends is attached to the boundary of the bulk spacetime. The body of the string extends along the radial direction and the free end of the string goes parallel to black hole horizon. The gauge/gravity duality suggests an identification between the end point of the string and the probe quark. Furthermore, the body of the string captures the effects of thermal plasma through which the external quark is moving. In this dual gravity picture, the string trails back and imparts a drag force on it's endpoint that is attached to the boundary. This drag force is obtained by calculating the rate of change in string momentum. The drag force is a function of temperature and chemical potential. The boundary gauge theory we are considering is on $\mathcal{M}^4$ described by the boundary coordinates t, x^1, x^2, x^3. The dynamics of a fundamental string is completely specified by the Nambu-Goto action in the black hole background within the string frame (2.5). On this background the world sheet action reads

$$S = -\frac{1}{2\pi\alpha'}\int d\tau d\sigma \sqrt{-\text{det}g_{\alpha\beta}}, \qquad g_{\alpha\beta} = \frac{\partial X^\mu}{\partial\sigma_\alpha}\frac{\partial X^\nu}{\partial\sigma_\beta}G_{\mu\nu}, \tag{4.1}$$

where $g_{\alpha\beta}$ is the induced metric on the world sheet and $G_{\mu\nu}$ is the background metric. The equation of motion derived from (4.1) is given by

$$\Delta_\alpha P^\alpha_\mu = 0, \qquad P^\alpha_\mu = -\frac{1}{2\pi\alpha'}G_{\mu\nu}\partial^\alpha X^\nu, \tag{4.2}$$

where Δ_α is the covariant derivative with respect to $g_{\alpha\beta}$ and P^α_μ is the world sheet current of space time energy-momentum of the test string. We consider the motion of the string along x^1. In the gauge, $\tau = t$ and $\sigma = z$, the string dynamics can be completely specified

by the function $x^1(t,z)$. In this case, the Lagrangian reads

$$\mathcal{L} = -\frac{1}{2\pi\alpha'}\sqrt{\frac{1}{H} + \frac{f(z)(\partial_z x^1)^2}{H} - \frac{(\partial_t x^1)^2}{Hf(z)}}, \tag{4.3}$$

where H is defined as

$$H = \sqrt{\frac{z^2}{\ell^2 e^{2A_s}}}. \tag{4.4}$$

To capture the dragged motion of the quark in the boundary theory we assume the following ansatz in the bulk [18]

$$x^1(t,z) = vt + \xi(z). \tag{4.5}$$

Here we have assumed only the late time behavior of the string motion. With this ansatz the Lagrangian reduces to

$$\mathcal{L} = -\frac{1}{2\pi\alpha'}\sqrt{\frac{1}{H} + \frac{f(z)(\partial_z \xi(z))^2}{H} - \frac{v^2}{Hf(z)}}. \tag{4.6}$$

The momentum which conjugates to $\xi(z)$ reads

$$\Pi_\xi = \frac{\partial \mathcal{L}}{\partial \xi'} = -\frac{\xi'}{2\pi\alpha'}\frac{f}{H}\sqrt{\frac{Hf}{f - v^2 + f^2\xi'^2}}. \tag{4.7}$$

For the sake of consistency it is important to invert the equation (4.7) and write it in the following way

$$\xi' = \sqrt{\frac{{\Pi_\xi}^2(f - v^2)}{\frac{f^2}{H^2}[\frac{1}{4\pi^2\alpha'^2}Hf - {\Pi_\xi}^2 H^2]}}. \tag{4.8}$$

Here the positive sign is taken due to the trailing nature of the string profile [18]. To obtain the string profile we have to solve the differential equation (4.8). To have a real $\xi(z)$, we further impose the constraints

$$\begin{aligned} f(z)|_{z=z_v} &= v^2, \\ {\Pi_\xi}^2|_{z=z_v} &= \frac{1}{4\pi^2\alpha'^2}\frac{v^2}{H}, \end{aligned} \tag{4.9}$$

so that one has $\xi'|_{z=z_v} = v^2/f^2$, keeping finite. The profile of the string is defined in the region with $z < z_v$, That is, there is a maximal value $z_v < z_h$ for the string profile.

The constraints are very useful to figure out the final form of the drag force. Before to compute the drag force, we here mention the relation between the drag force in the boundary field theory and the dissipation of momentum flowing down the string, in light of AdS/CFT correspondence. In the boundary theory the presence of the thermal medium results into dissipation of energy and momentum of external quark until it reaches thermal equilibrium with the medium. In the bulk theory the momentum is flowing down the string from the boundary to the bulk and the change of momentum at a given spatial point on the world sheet for a given time interval can be calculated. The identifications of the endpoint

of the string attached to the boundary with the quark and of the string in the bulk with the thermal medium around the quark suggest that the drag force can be realized in terms of the force imparted by the string on its boundary endpoint. To calculate the change of string momentum due to its motion along x_1 direction, we consider a closed curve on the world sheet and study how the momentum is conserved around this curve [53]. According

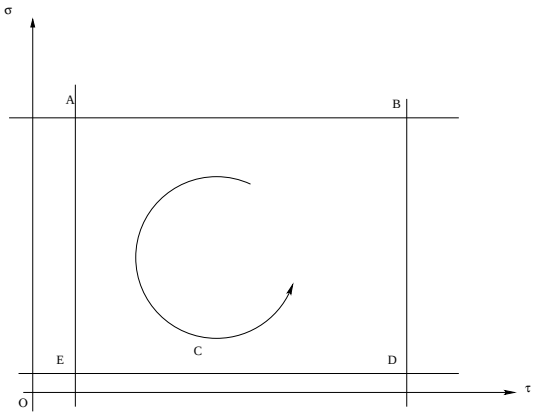

Figure 3. This plot shows a closed path in an anti-clockwise direction on a world sheet bounded by coordinates $[A = \tau_1, \sigma_2]$, $[B = \tau_2, \sigma_2]$, $[D = \tau_2, \sigma_1]$ and $[E = \tau_1, \sigma_1]$.

to the conservation of world sheet current of space time energy-momentum of the test string, the total flux calculated around the path C must be zero,

$$\oint_{ABDEA} (P^\tau_\mu d\sigma - P^\sigma_\mu d\tau) = 0. \tag{4.10}$$

Note that one end of the string is attached to the boundary and the other end close to horizon is free. In the static gauge, Eq. (4.10) reduces to

$$p^{t_1}_{x_1} - p^{t_2}_{x_1} = -\int_{t_2}^{t_1} \sqrt{-g} P^z_{x_1} dt, \tag{4.11}$$

where $p^t_{x_1}$ is the x_1 component of the total momentum at time t. Consequently the drag force is defined as

$$F_{drag} = \frac{dp_{x_1}}{dt} = -\sqrt{-g} P^z_{x_1} = -\frac{1}{2\pi\alpha'} \frac{\ell^2 e^{2A_s}}{{z_v}^2} v. \tag{4.12}$$

Finally we have to replace all the gravity parameters in terms of gauge theory parameters. Before doing that, we analyze the form of the constraints case by case. The exact forms of constraint for the solutions (3.9) and (3.15) are given respectively by

$$\begin{aligned} v^2 &= 1 - \tfrac{4V_{11}}{3}(3\sinh^4(\tfrac{z_v}{z_0}) + 2\sinh^6(\tfrac{z_v}{z_0})) + \tfrac{1}{8}V_{12}^2 \sinh^4\left(\tfrac{z_v}{z_0}\right), \\ v^2 &= 1 + \frac{1}{4g_g^2\ell^2}\left(\frac{\mu}{\int_0^{z_h} g(y)^{\frac{1}{3}} dy}\right)^2 \frac{\int_0^{z_v} g(x)\Big(\int_0^{z_h} g(r)dr \int_r^x g(y)^{\frac{1}{3}} dy\Big)dx}{\int_0^{z_h} g(x)dx} - \frac{\int_0^{z_v} g(x)dx}{\int_0^{z_h} g(x)dx}. \end{aligned} \tag{4.13}$$

It is always desirable to express the drag force in closed analytic form as a function of gauge theoretical variables. However it is very difficult to obtain analytic forms for the

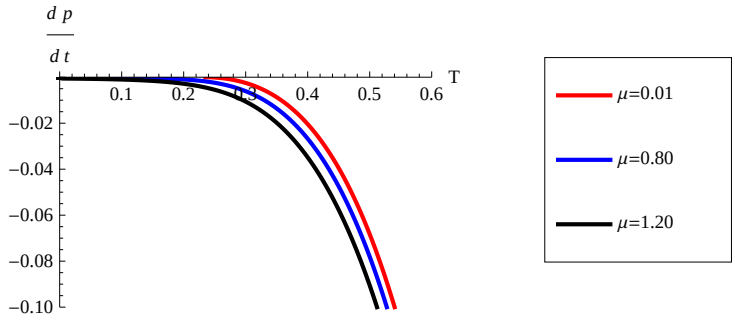

Figure 4. This plot shows the drag force from the analytic black hole solution as a function of T for chemical potential $\mu = 0.01, 0.80$, and 1.20 respectively. Here we take $v = 0.1$.

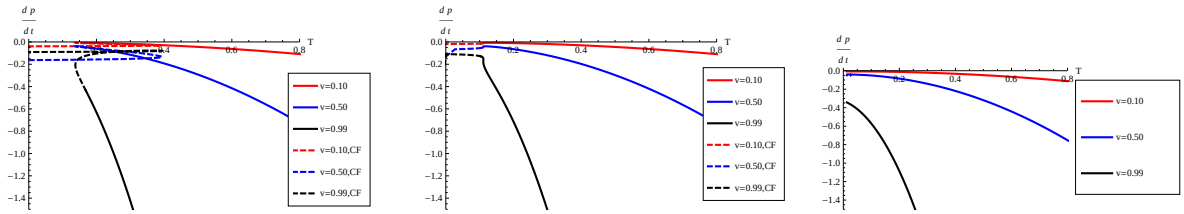

(a) (b) (c)

Figure 5. This figure shows the drag force as a function of T for the chemical potential $\mu = 0.10$ (plot a), 0.34 (plot b), and 0.80 (plot c), respectively, in the hQCD model. Here the dashed curves stand for the behavior of drag force in confined phase which is denoted by CF in the figure. In the confined phase, in fact the drag force is not well defined, meaning that the dashed curves do not make any sense here.

constraint (4.13) and the temperature (3.6). Instead we here solve them numerically and plot the drag force with respect to gauge theory parameters, e.g, temperature and chemical potential, so that the qualitative features of the drag force can be revealed.

Certainly the analytic black hole solution (3.9) does not dual to a QCD model. As a warm-up exercise, we plot the drag force in Figure [4] for a model dual to this black hole solution. We see that the drag force monotonically decreases with temperature and for a fixed temperature it becomes large as chemical potential grows. These features are qualitatively expected in realistic QCD. However, the behaviors of jet quenching parameter and screening length in the solution (3.9) are far away from QCD phenomenon and therefore we do not consider this solution from now on.

In Figure [5] we plot the drag force for our hQCD model given by the solution (3.15) with different chemical potentials $\mu = 0.10$, 0.34, and 0.80, respectively. We can see from the figure that for fixed chemical potential and temperature, the drag force increases with the velocity of the quark, while for fixed chemical potential and velocity, the drag force increases with temperature. These are expected features in QCD. In particular, let us note that in the low temperature region with small chemical potential, the drag force is a multi-valued function of temperature [see plot (a) and (b)], while it becomes a monotonic

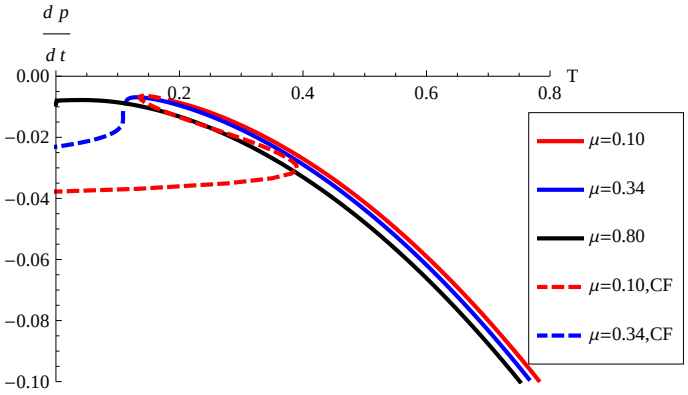

Figure 6. The figure shows the drag force as a function of T for three chemical potential $\mu = 0.10, 0.34$, and 0.80, respectively in the hQCD model. The dashed parts of the curves stand for the drag force in the confined phase which denoted by CF in the figure. Here we take $v = 0.1$.

function with large chemical potential [see plot (c)]. This feature is closely related to the confinement/deconfinement phase transition in this hQCD model [15]. The dashed parts of curves in plot (a) and (b) denote the drag force in the confined phase and actually they do not make any sense here since drag force is not well-defined in the confined phase. Our result for the drag force in the deconfined phase is in agreement with the one in [54]. For comparison, in Figure [6] we plot the drag force versus temperature with three different chemical potentials $\mu = 0.10$, 0.34 and 0.80, respectively. In this figure the velocity of quark is taken as $v = 0.1$.

5 Jet Quenching parameter

In this section, we use the AdS/CFT duality to compute the jet quenching parameter in our hQCD model. The holographic method to compute this quantity needs a consideration of Wilson loop ($\mathcal{C}$) traced out by a $q\bar{q}$ pair [33]. The Wilson loop is taken to lie along the light cone in the gauge theory. The gravity dual of this $q\bar{q}$ pair is represented as the two end points of a fundamental string, attached to the boundary of the bulk spacetime. Body of the string hangs along the radial direction and up to the horizon of aAdS black hole. The Wilson loop is mapped, in the dual theory, as the string world sheet. The jet quenching parameter ($\hat{q}$) is related to the thermal expectation value of the light-like Wilson loop operator, $\langle \mathcal{W}(\mathcal{C}_{light-like})\rangle$ [55]. The holographic correspondence between thermal expectation value of the light-like Wilson loop operator in fundamental representation $\langle \mathcal{W}^F(\mathcal{C}_{light-like})\rangle$ and the exponential of the worldsheet action, e^{-S}, leads us to obtain a working formula of $\hat{q}$ in dual gravity theory. Here, S stands for the worldsheet action of the fundamental string.

$$\langle \mathcal{W}^F(\mathcal{C}_{light-like})\rangle = \exp[-S(\mathcal{C})]. \tag{5.1}$$

In the planar limit, considering the fact $Tr_{Adj} = Tr^2_{Fund}$, the relation between $W^F(\mathcal{C})$ and $W^A(\mathcal{C})$ can be easily established as

$$\langle W^A(\mathcal{C})\rangle = \langle W^F(\mathcal{C})\rangle^2. \tag{5.2}$$

Now we start with the background black hole solution in string frame

$$ds^2_S = \frac{\ell^2 e^{2A_s}}{z^2}\left(-f(z)dt^2 + \frac{dz^2}{f(z)} + dx^1dx^1 + dx^2dx^2 + dx^3dx^3\right). \tag{5.3}$$

By introducing the light cone coordinates defined as

$$x^{\pm} = \frac{t \pm x^1}{\sqrt{2}}, \tag{5.4}$$

the black hole metric (5.3) can be rewritten as

$$\begin{aligned} ds^2_S = & \frac{\ell^2 e^{2A_s}}{z^2}\left(\frac{(1-f(z))}{2}((dx^+)^2 + (dx^-)^2) - (1+f(z))(dx^+dx^-)\right. \\ & \left. + \frac{dz^2}{f(z)} + dx^2dx^2 + dx^3dx^3\right). \end{aligned} \tag{5.5}$$

We take the gauge with $\tau = x^-(0 \le x^- \le L^-)$, $\sigma = x^2(-\frac{L_2}{2} \le x_2 \le \frac{L_2}{2})$, and set the pair of quarks at $x^2 = \pm\frac{L_2}{2}$ on $x^+ =$ constant, $x^3 =$ constant plane. In the limit with $L^- \gg L_2$ the string profile is completely specified by $z = z(\sigma)$. Following [33], using (5.1), (5.2), one has

$$\langle W^A(\mathcal{C})\rangle = \exp(-\frac{1}{4\sqrt{2}}\hat{q}L^-L_2^2), \tag{5.6}$$

where the jet quenching parameter is defined as

$$\hat{q} = \frac{8\sqrt{2}(S - S_0)}{L^-\ell^2}, \tag{5.7}$$

where S is the Nambu-Goto action of the string and S_0 is the self energy from the mass of two quarks.

Substituting the induced metric of the fundamental string into the Nambu-Goto action (4.1), we get

$$\begin{aligned} S &= -\frac{1}{2\pi\alpha'}\int d\tau d\sigma \sqrt{-\det g_{\alpha\beta}}, \\ &= \frac{L^-\ell^2}{\sqrt{2}\pi\alpha'}\int_0^{\frac{L_2}{2}} d\sigma \frac{e^{2A_s}}{z^2}\sqrt{(1-f(z))(1+\frac{z'^2}{f(z)})}. \end{aligned} \tag{5.8}$$

Since the integrand in (5.8) does not explicitly depend on σ, one can regard σ as time and the integrand as a Lagrangian. In this case the corresponding Hamiltonian is conserved. That is, we can have

$$\frac{\partial\mathcal{L}}{\partial z'}z' - \mathcal{L} = E, \tag{5.9}$$

where E is a constant and $\mathcal{L}$ is the integrand in (5.8). From this relation we obtain the equation of motion for z as

$$z'^2 = f(z)(\frac{e^{4A_s}}{z^4}\frac{(1-f(z))}{E^2} - 1). \tag{5.10}$$

We choose the boundary conditions $z(\pm\frac{L_2}{2}) = 0$ and $z^{'}(0) = 0$. In that case, the turning point z_T is determined by solving Eq.(5.10). Since $z^{'}(\sigma)$ is a real function, so the square of it should be non-negative. The realization of boundary condition $z^{'}(0) = 0$ at the turning point requires the proper choices of zeros and the positivity region of the right hand side of Eq.(5.10). From the boundary conditions of the black hole solution

$$\lim_{z\to z_h} f(z) = 0, \quad \lim_{z\to 0} f(z) = 1, \tag{5.11}$$

together with the fact that we are interested in the case with small E, it is clear that the factor $\frac{e^{4A_s}(1-f(z))-E^2z^4}{E^2z^4}$ is always positive near the black hole horizon and negative near the boundary. To remove the region with a negative $z^{'2}$, we consider a modified boundary at $z = \delta$. We assume that at $z = z_{min}$,

$$\frac{e^{4A_s(z_{min})}}{z_{min}^4}\frac{(1-f(z_{min}))}{E^2} - 1 = 0, \tag{5.12}$$

and $\delta > z_{min}$. In the region $\delta \le z \le z_h$, thus, the factor $[\frac{e^{4A_S}}{z^4}\frac{(1-f(z))}{E^2} - 1]$ is always positive. So only viable solution of $z^{'2} = 0$ is

$$f(z) = 0 \Rightarrow z_T = z_h. \tag{5.13}$$

That is, the turning point is just at the horizon. The distance between two quarks can be determined by

$$\frac{L_2}{2} = \int_\delta^{z_h} dz \frac{E}{\sqrt{f[e^{4A_s}(1-f)z^{-4} - E^2]}}. \tag{5.14}$$

As we are interested in the small L_2 limit, considering the smallness of E, we can expand Eq.(5.14) in terms of E as

$$\frac{L_2}{2E} = \int_\delta^{z_h} dz \frac{z^2 e^{-2A_s}}{\sqrt{f(1-f)}} + \frac{E^2}{2}\int_\delta^{z_h} dz \frac{e^{-6A_s}z^6}{\sqrt{f(1-f)^3}} + \mathcal{O}(E^4). \tag{5.15}$$

Inverting (5.15) suitably, we can obtain E up to the leading order of L_2 as

$$E = \frac{L_2}{2\int_\delta^{z_h} dz \frac{z^2 e^{-2A_s}}{\sqrt{f(1-f)}}} + \mathcal{O}({L_2}^3). \tag{5.16}$$

Thus we can obtain the string action

$$S = \frac{L^-\ell^2}{\sqrt{2}\pi\alpha'}\int_\delta^{z_h} dz \frac{e^{4A_s}(1-f)}{z^2\sqrt{f(e^{4A_s}(1-f) - z^4E^2)}}. \tag{5.17}$$

Clearly this action is divergent. The divergence comes from the contribution of mass of two quarks. With the gauge $x^- = \tau$ and $z = \sigma$, the self energy of two free quarks reads

$$S_0 = \frac{L^- \ell^2}{\sqrt{2}\pi\alpha'} \int_\delta^{z_h} dz \frac{e^{2A_s}}{z^2} \sqrt{\frac{(1-f)}{f}}. \tag{5.18}$$

Thus the regularized action up to the leading order of L_2 is given by

$$S_I = S - S_0 = \frac{L^- L_2^2 \ell^2}{8\sqrt{2}\pi\alpha'} \frac{1}{\int_\delta^{z_h} dz \frac{z^2 e^{-2A_s}}{\sqrt{f(1-f)}}} + \mathcal{O}({L_2}^4). \tag{5.19}$$

With the definition of the jet quenching parameter (5.7), we finally reach

$$\hat{q} = \frac{\ell^2}{\pi\alpha'} \frac{1}{\int_\delta^{z_h} dz \frac{z^2 e^{-2A_s}}{\sqrt{f(1-f)}}}. \tag{5.20}$$

In fact the cutoff here can be removed by noting the fact that the integrand is regular inside the region $0 \leq z \leq z_h$, i.e, from the horizon to the real boundary,

$$\int_\delta^{z_h} dz \frac{z^2 e^{-2A_s}}{\sqrt{f(1-f)}} = \int_0^{z_h} dz \frac{z^2 e^{-2A_s}}{\sqrt{f(1-f)}} - \int_0^{\delta} dz \frac{z^2 e^{-2A_s}}{\sqrt{f(1-f)}}. \tag{5.21}$$

The second integral in the right hand side of the above equation smoothly vanishes in the limit $\delta \to 0$. So the final expression for the jet-quenching parameter is

$$\hat{q} = \frac{\ell^2}{\pi\alpha'} \frac{1}{\int_0^{z_h} dz \frac{z^2 e^{-2A_s}}{\sqrt{f(1-f)}}}. \tag{5.22}$$

Because the black hole metric is still too complicated to obtain an analytical expression of the jet-quenching parameter in terms of physical parameters, we plot in Figure [7] the jet-quenching parameter as a function of temperature in the hQCD model with three chemical potentials $\mu = 0.10$, 0.34 and 0.80, respectively. For large $\mu \geq \mu_c$ cases, the jet-quenching parameter decreases monotonically with temperature, which agrees with the one in [56] qualitatively. On the other hand, when $\mu < \mu_c$, the jet-quenching parameter is a multi-valued function of temperature in low temperature region and it decreases monotonically with respect to temperature in high temperature region. The multi-valued behavior of the jet-quenching parameter in low temperature region is clearly related to the first order phase transition between hadron phase (confined phase) and QGP phase (deconfined phase). The jet-quenching parameter confirms the hydrodynamical description of QGP phase and agrees with the real QCD expectation in high temperature. Once again, as the drag force in the confined phase, the dashed parts of curves in Figure [7] denote the jet-quenching parameter in the confined phase and thus they do not make any sense.

6 Hot plasma wind and screening length

The screening length is defined as the maximum length achieved by a quark-antiquark bound state at temperature $T > T_c$, beyond which the pair dissociates. For quark-antiquark

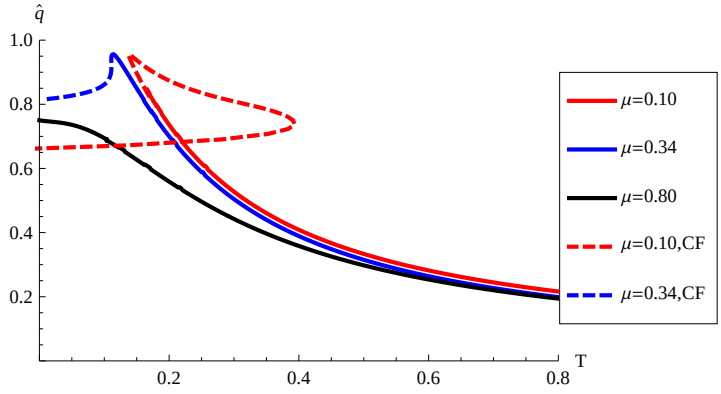

Figure 7. The figure shows the jet-quenching parameter as a function of T for three chemical potentials $\mu = 0.10, 0.34$, and 0.8, respectively, in the hQCD model. The dashed parts of curves stand for the jet-quenching parameter in the confined phase which are denoted by CF in the figure.

pair, the energetically favorable configuration in the dual gravity theory is a fundamental string with both ends attached to the boundary. The attached endpoints correspond to the $q\bar{q}$ pair whereas being separated beyond the screening length, thus dissociated from each other, the pair maps into two separate strings hanging from the boundary. In [53], the screening length is computed in the rest frame of $q\bar{q}$ pair and the plasma wind flows at a constant speed v for the hot $\mathcal{N} = 4$ SYM plasma. This setup is identified with a quark-antiquark pair moving in hot $\mathcal{N} = 4$ SYM plasma. In this section, we compute the screening length for the hQCD model (3.15) in the same way as in [53].

In the static frame of $q\bar{q}$ pair, we assume that the hot plasma is moving with velocity v in the negative x_3 direction. The Wilson loop we are interested in lies in the $t - x_1$ plane specified by the length $\mathcal{T}$ and L respectively. We assume $\mathcal{T} \gg L$ such that the string world sheet is invariant under translation along the time direction. The boost we are considering is defined as

$$\begin{aligned} dt &= \cosh\eta dt^{'} - \sinh\eta dx_3^{'}, \\ dx_3 &= -\sinh\eta dt^{'} + \cosh\eta dx_3^{'}, \end{aligned} \tag{6.1}$$

where $\cosh\eta = \gamma$, $\sinh\eta = \gamma v$ and $\gamma = 1/\sqrt{1-v^2}$ is the Lorentz boost factor. With the Lorentz transformation, we obtain the boosted black hole metric in string frame

$$\begin{aligned} ds_S^2 = H(z)[&-(1-(1-f)\cosh^2\eta)dt^2 + (1+(1-f)\sinh^2\eta)(dx^3)^2, \\ &-2(1-f)\cosh\eta\sinh\eta dt dx^3 + (dx^1)^2 + (dx^2)^2 + \frac{dz^2}{f(z)}], \end{aligned} \tag{6.2}$$

where $H(z) = \ell^2 e^{2A_s}/z^2$. We prefer to work in the static gauge

$$\tau = t, \sigma = x^1, x^2(\sigma) = x^3(\sigma) = \text{constant}, \tag{6.3}$$

with the following boundary conditions

$$z(\sigma = \pm\frac{L}{2}) = 0, z(\sigma = 0) = z_c, z^{'}(\sigma = 0) = 0. \tag{6.4}$$

Thus the world sheet metric induced on the boosted background is given as

$$\begin{aligned} g_{\tau\tau} &= -H(z)(1-(1-f)\cosh^2\eta), \\ g_{\tau\sigma} &= g_{\sigma\tau} = 0, \\ g_{\sigma\sigma} &= H(z)[1+(1+\frac{z'^2}{f(z)})]. \end{aligned} \tag{6.5}$$

Then the Nambu-Goto action for the string takes the form as

$$S = -\frac{\mathcal{T}}{\pi\alpha'}\int_0^{\frac{L}{2}} d\sigma H(z)\sqrt{(1-(1-f)\cosh^2\eta)(1+\frac{z'^2}{f})}. \tag{6.6}$$

As the Lagrangian $\mathcal{L}$ in (6.6) does not depend on σ explicitly, the corresponding Hamiltonian is conserved and can be viewed as a constant of motion

$$-q = \frac{\partial\mathcal{L}}{\partial z'}z' - \mathcal{L}. \tag{6.7}$$

With this we can cast the equation of motion in the form as

$$z' = \frac{\sqrt{f[H^2(1-(1-f)\cosh^2\eta)-q^2]}}{q}. \tag{6.8}$$

It is evident from the constraint (6.8) that at the horizon, $z = z_h$, where $f(z_h) = 0$, the factor $\frac{H^2}{q^2}(1-(1-f)\cosh^2\eta)-1 = -\frac{H^2}{q^2}\sinh^2\eta - 1$ is always negative. At the boundary, $f(0) = 1$, the factor $\frac{H^2}{q^2}(1-(1-f)\cosh^2\eta)-1 = \frac{H^2}{q^2}-1$ is always positive for small values of $q < H$. Therefore in the range $0 < z < z_h$ there must be a location ($z = z_c$) where $\frac{H^2}{q^2}(1-(1-f)\cosh^2\eta)-1$ switches its sign. Accordingly $z = z_c$ is the physical turning point of the string configuration. The string can not be stretched up to the horizon as z' is an imaginary quantity in the region $z_c < z < z_h$. By solving the equation

$$\frac{f(z_c)H^2(z_c)\cosh^2\eta}{q^2} - \frac{H^2(z_c)\sinh^2\eta}{q^2} - 1 = 0, \tag{6.9}$$

the turning point can be numerically determined. Then one can obtain the binding energy between the quark and antiquark pair through calculating the action (6.6) with constraint (6.8)

$$V = -\frac{S-S_0}{\mathcal{T}}, \tag{6.10}$$

where S_0 is given by

$$S_0 = -\frac{\mathcal{T}}{\pi\alpha'}\int_0^{z_c} dz\sqrt{-G_{tt}G_{zz}}. \tag{6.11}$$

The distance between quark and antiquark can be calculated from (6.8) as

$$\frac{L}{2q} = \int_0^{z_c} dz \frac{1}{H\sqrt{f[(1-\cosh^2\eta(1-f))-\frac{q^2}{H^2}]}}. \tag{6.12}$$

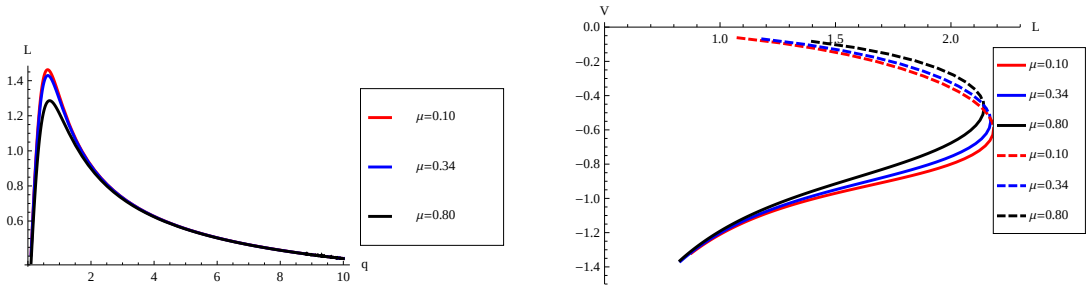

(a) (b)

Figure 8. Plot (a) shows the quark-antiquark distance as a function of q for a fixed rapidity, while plot (b) shows the binding energy with respect to the distance. In both plots we fix the chemical potential $\mu = 0.10, 0.34$, and 0.80, respectively. We have set a same temperature T to obtain these curves.

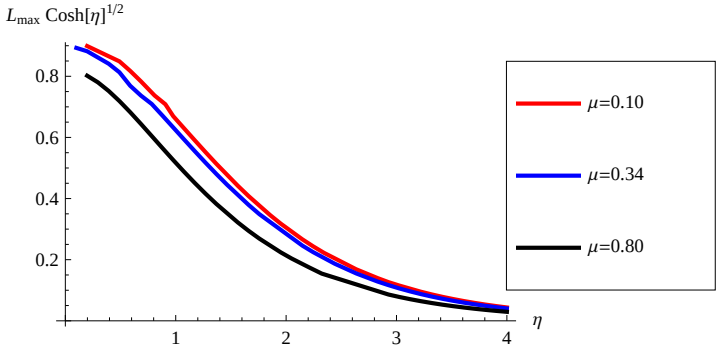

Figure 9. The screening length versus the rapidity η for the cases $\mu = 0.1, 0.34$, and 0.8, respectively. We have set a same temperature T to obtain these curves.

It is not possible to work out the integration in (6.12) explicitly. To determine the screening length, we plot the distance L with respect to the constant of motion q for a fixed rapidity η in Figure [8] (see plot (a)). It turns out that for a fixed value of rapidity, there exists a maximum for L, which is regarded as the screening length $L_s = L_{max}(\eta)/(\pi T)$. Plot (b) in Figure [8] shows the binding energy V given by (6.10) with respect to L. One can see from plot (a) that the quark-antiquark distance starts from zero when q is also zero, it increases sharply with respect to q, reaches its maximum at a certain q, and then decreases monotonically to zero at some finite q. In between these two zeros, there exists a single $L = L_{max}$ beyond which there is no solution of Eq.(6.12). This implies the quark-antiquark pair dissociates beyond $L = L_{max}$. We identify $L_{max}(\eta)/(\pi T)$ with the screening length L_s. For the $\mu = 0.1$ case, $L_{max} \simeq 1.4$ and $L_s \simeq 1.4/(\pi T) \simeq 0.45/T$, close to the lattice calculation $L_s \sim 0.5/T$ [57] of the static potential between heavy quark and antiquark in QCD. Plot (b) shows that there are two branches for the binding energy in the region $L < L_{max}$. The branch with dashed curves has a higher energy than the one with solid curves. This implies that the branch with dashed curves is physically disfavored.

The screening length $L_s(\eta)$ as a function of rapidity can be obtained numerically as

illustrated in Figure [9]. One finds that it decreases with velocity which indicates that the quark-antiquark pair dissociates at a lower temperature as it is moving. This behavior is also observed in [54]. If the qualitative behavior holds for QCD, it will have the consequence for quarkonium suppression in heavy ion collision. Additionally, our results show that the case with smaller chemical potential has a larger screening length.

7 Free energy and phase transition

In this section, we would like to calculate the free energy of the black hole solution dual to the hQCD model by following [46]. Ref. [46] studies the free energy of a generic Einstein-Maxwell-Dilaton system. The system considered in [46] is given by

$$\begin{aligned} I &= M_P^{d-1}\int_M d^{d+1}x\sqrt{-g}\left[R-\tfrac{Z(\Phi)}{4}F^2-\tfrac{1}{2}(\partial\Phi)^2+V(\Phi)\right]+I_{GH}\ , \\ I_{GH} &= 2M_P^{d-1}\int_{\partial M} d^dx\sqrt{-h}K\ , \end{aligned} \tag{7.1}$$

with following ansatz

$$ds^2 = e^{2\tilde{A}(u)}\left(-\tilde{f}(u)dt^2+dx^idx^i\right)+\frac{du^2}{\tilde{f}(u)}\ ,\quad \mathbf{A}=A_t(u)dt\ ,\quad \Phi=\Phi(u)\ , \tag{7.2}$$

where M_P is the Planck mass, and K is the extrinsic curvature of the finite boundary ∂M with induced metric h. By the following transformations

$$\begin{aligned} \frac{d}{du} &= e^{-\tilde{A}(u(z))}\frac{d}{dz},\quad \frac{d^2}{du^2} = e^{-2\tilde{A}(u(z))}\Big(\frac{d^2}{dz^2}-\frac{d\tilde{A}(u(z))}{dz}\frac{d}{dz}\Big),\quad \tilde{f}(u(z))=f(z), \\ \Phi(u) &= \sqrt{\frac{8}{3}}\phi(z),\quad Z(\Phi)=1,\quad d=4,\quad M_P^{d-1}=\frac{1}{16\pi G_5}, \\ \tilde{A}(u(z)) &= A_e(z)-\log(z),\quad -V(u(z))=V_E(z), \end{aligned} \tag{7.3}$$

we can change the system and ansatz to ours discussed in this paper. Here we have chosen $\tilde{A}(u(z)) = A_e(z)-\log(z)$ as a gauge. Varying the action (7.1) yields equations of motion for the gravitational field

$$E_{\mu\nu}+\frac{1}{2}g_{\mu\nu}\left(\frac{1}{2}\partial_\mu\Phi\partial^\mu\Phi-V(\Phi)\right)-\frac{1}{2}\partial_\mu\Phi\partial_\nu\Phi-\frac{Z(\Phi)}{2}\left(F_{\mu\rho}F^\rho_\nu-\frac{1}{4}g_{\mu\nu}F_{\rho\sigma}F^{\rho\sigma}\right)=0 \tag{7.4}$$

The Maxwell equation and the explicit forms of Einstein equations read

$$\frac{d}{du}\left(e^{(d-2)\tilde{A}}Z\dot{A}_t\right) = 0\ , \tag{7.5a}$$

$$2(d-1)\ddot{\tilde{A}}+\dot{\Phi}^2 = 0\ , \tag{7.5b}$$

$$\ddot{\tilde{f}}+d\dot{\tilde{A}}\dot{\tilde{f}}-e^{-2\tilde{A}}Z\dot{A}_t^2 = 0\ , \tag{7.5c}$$

$$(d-1)\dot{\tilde{A}}\dot{\tilde{f}}+\left(d(d-1)\dot{\tilde{A}}^2-\frac{1}{2}\dot{\Phi}^2\right)\tilde{f}-V+\frac{1}{2}Ze^{-2\tilde{A}}\dot{A}_t^2 = 0\ , \tag{7.5d}$$

where an over dot stands for the derivative with respect to u. Eq.(7.5a) is the Maxwell equation and the other three Eq.(7.5b) (7.5c) (7.5d) are obtained from Einstein equations.

One can easily check that Eq.(7.5b) and Eq.(7.5c) correspond to Eq.(2.8) and Eq.(2.9), respectively. In addition, the equation of motion for the scalar field is

$$\frac{1}{\sqrt{-g}}\partial_u\left(\sqrt{-g}\partial_u\Phi\right)+V'(\Phi)-\frac{Z'(\Phi)}{4}F^2=0, \tag{7.6}$$

where the prime denotes the derivative with respect to Φ. From (7.5a), one obtains

$$A_t(u)=\mu+\int_{u_0}^{u}\frac{\rho}{e^{(d-2)\tilde{A}(\tilde{u})}Z(\Phi)}d\tilde{u}, \tag{7.7}$$

where μ and ρ are the chemical potential and charge density of the black hole solution, respectively, and u_0 stands for the UV boundary.

By defining the superpotential W in the following way [46]

$$\dot{\Phi}=W'(\Phi), \tag{7.8}$$

the equation (7.5b) can be solved as

$$\dot{\tilde{A}}=-\frac{W(\Phi)}{2(d-1)}\ . \tag{7.9}$$

Equivalently,

$$\tilde{A}(\Phi)=\tilde{A}_0-\frac{1}{2(d-1)}\int_{\Phi_0}^{\Phi}\delta\tilde{\Phi}\,\frac{W(\tilde{\Phi})}{W'(\tilde{\Phi})}\ ,\quad u=u_0+\int_{\Phi_0}^{\Phi}\frac{\delta\tilde{\Phi}}{W'(\tilde{\Phi})}, \tag{7.10}$$

where $\tilde{A}_0=\tilde{A}(\Phi_0)$, $\Phi(u=u_0)=\Phi_0$.

The temperature $\tilde{T}$ associated with the black hole in metric (7.2) is given by

$$\tilde{T}=\frac{1}{4\pi}\left|e^{\tilde{A}}\dot{\tilde{f}}\right|_{u=u_h}, \tag{7.11}$$

where u_h denotes the black hole horizon. The entropy density for the black hole solution (7.2) is

$$\tilde{S}=4\pi e^{(d-1)\tilde{A}(\Phi_h)}=4\pi e^{(d-1)\tilde{A}_0-\frac{1}{2}\int_{\Phi_0}^{\Phi_h}\delta\tilde{\Phi}\frac{W}{W'}},\quad (\Phi_h:=\Phi(u_h)). \tag{7.12}$$

where $M_P^{d-1}=1$ has been taken.

The on-shell action I has a bulk contribution I_E and a boundary contribution I_{GH} from the Gibbons-Hawking term. Here we evaluate it with an UV cutoff at $u=u_0$ or $z=\epsilon$. A standard computation gives us with the action density

$$I_{on-shell}=\tilde{T}^{-1}(-W+\dot{\tilde{f}})e^{d\tilde{A}(u_0)}|_{u=u_0}. \tag{7.13}$$

With the equations (7.3)(7.5c) and $A_t(u_h)=0$, the free energy density is found to be

$$\begin{aligned}F&=-e^{d\tilde{A}_0}W(\Phi_0)-\tilde{T}\tilde{S}+\rho^2\int_{\Phi_h}^{\Phi_0}\frac{d\tilde{\Phi}}{e^{(d-2)\tilde{A}}Z(\Phi)W'(\Phi)},\\&=6b^3(z)\frac{d}{dz}\Big(A_e(z)-\log(z)\Big)\Big|_{z=\epsilon}-TS+\frac{\mu^2}{\int_{z_h}^{\epsilon}\frac{dz}{b(z)Z(\phi)}}\ ,\end{aligned} \tag{7.14}$$

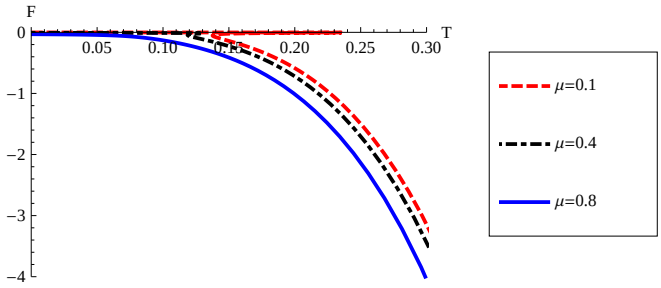

Figure 10. The free energy of the background black hole solution with respect to temperature. It shows that in the small $\mu < \mu_c$ case, the free energy has a multi-valued behavior, while it is absent in the large $\mu \geq \mu_c$ case. The parameters $\ell = 1, 16\pi G_5 = 1, g_g = 1, k = 0.3\text{GeV}$ are taken here.

where $b(z) = e^{A_e(z)}/z$. Note that in the second line of Eq.(7.14), we have considered the case $d = 4$ and the expression of the free energy is written in the ansatz (2.6) in Einstein frame. The first term in Eq.(7.14) corresponds to the black hole mass and the last term can be expressed as $-\mu\rho$.

With the analytical result (7.14), one can obtain the free energy of the black hole solution (3.15) with respect to temperature with various chemical potentials numerically. Figure [10] shows the free energy density of the black hole solution. It can be seen that the free energy density is a multi-valued function of temperature in the case $\mu < \mu_c$ and it becomes monotonically in the large μ region $\mu > \mu_c$. The multi-value behavior of the free energy indicates the existence of a first order phase transition in the small μ region.

To clearly see this, it should be helpful to recall the temperature behavior of the black hole (see Figure [2]). One can see that when $\mu > \mu_c$, the black hole is always stable with positive heat capacity. When $\mu < \mu_c$, one can see from plot (b) that as $T > T_M$, the black hole is also always stable with positive heat capacity (in branch 1), when $0 < T < T_m$, the black hole is also stable with positive heat capacity (in branch 3), while when $T_m < T < T_M$, there exist three black hole solutions with a same temperature. For instance, for temperature T_p, there exist three black hole solutions with horizon radii z_p', z_p and z_p'', in branch 1, 2 and 3, respectively. The black hole solutions in branch 2 are unstable because those black holes have negative heat capacity. We call black holes in branch 1 and branch 3 as large and small black holes, respectively, when $T_m < T < T_M$, because the black holes in branch 1 have large horizon radius and entropy, while the black holes in branch 3 have small horizon radius and entropy. From Figure [2,10], we can see that when $\mu > \mu_c$, the black hole solution always dominates, which indicates the dual field theory is in deconfined phase, while in the $\mu < \mu_c$ regime, when $T_m < T < T_M$, there exists a phase transition between large black hole and small black hole. In this transition, the entropy has a jump, which means this is a first order phase transition. On the other hand, when $0 < T < T_m$, the small black hole solution in branch 3 is dominated. This is quite different from the case of Schwarzschild black hole in AdS space. There when temperature is less than a certain value, there does not exist black hole solution. In this case, the thermal gas is dominated. Above a certain temperature, there exist two black hole

solutions, one is stable and the other is unstable. Therefore there exists a well-known first order phase transition (Hawking-Page phase transition) between black hole and thermal gas in AdS space [47]. This transition is explained as the confinement/deconfinement phase transition of dual field theory. In our case even in the low temperature regime with $T < T_m$, the small black hole is dominated, the free energy for these small black holes is negative. Compared to thermal gas, those black hole solutions are still favored. When temperature increases beyond T_m, the black hole solution with large horizon radius in branch 1 is favored than the one with small horizon radius in branch 3. In this case, a phase transition happens. Since the entropy of small black holes in branch 3 is much small than the one of large black holes in branch 1, this phase transition therefore can be identified as the confinement/deconfinement phase transition in the dual theory. Of course, this phase transition is not same as the Hawking-Page phase transition. The free energy calculation further confirms this picture. And this picture is completely consistent with the one in [15] by computing heavy quark potential in this model. In addition, we would like to stress that the phase transition between large black hole and small black hole is the same as the one found in [52], but the transition in our case is in grand canonical ensemble, while the one in [52] is in canonical ensemble. As a result, $T - Q$ phase diagram in Figure 1 of [52] is similar to our $T - \mu$ phase diagram.

In a word, in the small μ region there exists a first order phase transition, while it is absent in the large μ region through studying the free energy of the system. The existence of the first order phase transition in the small μ region is consistent with the analysis of Wilson loop in this black hole background [15]. The existence of the critical point at $\mu = \mu_c$ is in agreement with recent lattice calculation given in [58]. Let us notice that in [15] we claim that there is a crossover or higher order phase transition in the large $\mu > \mu_c$ region, while the free energy calculation here shows no such phase transition. In this sense, free energy may show less information about phase transition and one should take more probes into considerations, such as Polyakov loop [15], to understand the phase structure completely. These two conclusions are in fact not in contradiction with each other. The reason is as follows. The free energy calculation here only concerns with the black hole background, from the point of view of QCD, the black hole background does not include the degrees of freedom of quarks, while the Wilson loop calculation in [15] is related to the dynamics of quarks.

In Figure [11] we plot the phase diagram of the hQCD model. The difference between the confinement/deconfiement phase transition lines come from the different consideration as mentioned above.

At the end of this section, let us stress the question whether there exists the so-called Hawking-Page phase transition between black hole and thermal gas in our model. Note that in the above analysis, our phase transition happens between small black hole and large black hole in the region with small chemical potential $\mu < \mu_c$, such a transition does not occur as $\mu > \mu_c$. It is therefore of some interest to investigate whether there exists any transition between black hole solution and thermal gas solution in our hQCD model. For this aim, we have to first find the thermal gas solution. Unfortunately, in this potential reconstruct approach, to find out the thermal gas solution is not an easy job since we

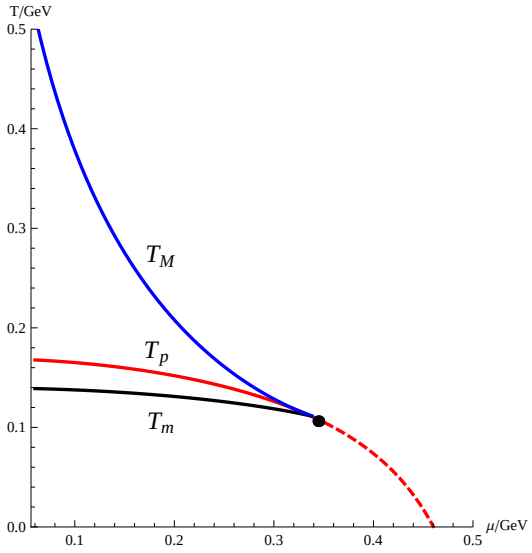

Figure 11. The phase diagram of the hQCD model. The red and dashed red curves are obtained in [15] through studying VEV of Polyakov loop. The two curves stand for first order and continuous phase (or second order) transition respectively. The thick black and blue curves correspond to the minimal temperature T_m and maximal temperature T_M in small μ region. The thick black curve is obtained by calculating the free energy. The black dot denotes the critical point. T_p denotes the transition temperature.

have not an explicitly analytic form of the potential for the dilaton field in our hQCD model. But even so, we still can make some arguments which lead to the conclusion that there does not exist any phase transition between black hole and thermal gas solutions in the hQCD model. The main reason for this comes from the fact that in the hQCD model, for any temperature, there exist corresponding black hole solutions. This can be seen from Figure [2]. It shows in plot (a) that when $\mu > \mu_c$, the black hole temperature increases monotonically from zero with the smallest black hole radius, which corresponds to an extremal black hole, while when $\mu < \mu_c$, plot (b) shows that as $T \leq T_m$, there exists a region with stable black holes with small horizon radius, including the extremal black hole; and as $T > T_m$, there exists the region with stable black holes with larger horizon radius. In addition, for a given temperature, it is generally believed that the black hole solution has much large entropy than the thermal gas, so that the black hole phase is always dominated. As a result, whatever the chemical potential is, the black hole solutions are always dominated over the thermal gas solutions. This is quite different from the case of Schwarzschild-AdS black hole. In the latter case, there exists a minimal temperature, below which there is no black hole solution. This leads to the conclusion that in low temperature the thermal gas solution is favored, while in high temperature the black hole solution is dominated, and thus there must exist the Hawking-Page phase transition between the black hole solution and thermal gas solution at a certain temperature. Therefore in our case, black hole solutions are always dominated and there does not exist any phase transition between black hole solution and thermal gas solution. This might be a common feature for black

hole solutions with Ricci flat horizon in AdS space. But as we analyzed above, there exists indeed the phase transition between small black hole and large black hole in our model with $\mu < \mu_c$. This phase transition can also be understood as the confinement/deconfinement phase transition in QCD since clearly the small black hole has a much less entropy than the large one. And this interpretation is also consistent with the calculation of heavy quark potential in [15].

8 Conclusion and discussion

In this paper, we have continued to study the holographic QCD model proposed in [15], in an Einstein-Maxwell-Dilaton system. At first we have generalized case with a non-minimal coupling between Maxwell field and dilaton field, and given a generic formulism for generating a set of exact and asymptotic AdS black hole solutions in the EMD system. After briefly reviewing the main features of the hQCD model, we have studied some aspects of QGP phase of the hQCD model by calculating some quantities such as drag force, jet quenching parameter and screening length. The calculations show that the behaviors of those quantities are consistent with the expectation from realistic QCD.

It is found that the drag force increases monotonically with temperature which is quite good consistent with real QCD phenomenon in the larger chemical potential region with $\mu \geq \mu_c$. In the small chemical region with $\mu < \mu_c$, the drag force also monotonically increases in the high temperature region, while in the low temperature, it shows a multi-valued behavior. Note that in the case $\mu < \mu_c$, the solution is dual to the confined phase of QCD. In that case, the drag force is not well defined. Therefore the change from the multi-valued behavior to the monotonic behavior just manifests the existence of the first order phase transition. The jet quenching parameter has monotonically decreasing behavior versus temperature, which is also consistent with QCD experiments in $\mu \geq \mu_c$. For the $\mu < \mu_c$ case, the jet quenching parameter agrees with real QCD expectation in high temperature and once again, it shows the multi-valued behavior in the low-temperature region. As in the case of drag force, the multi-valued behavior of jet quenching parameter in the low temperature region is consistent with the existence of first order phase transition in this hQCD model. For the screening length we have plotted the separation between quark and anti-quark with respect to the constant of motion q. It is clear from the plot that for both cases when $\mu \geq \mu_c$ and $\mu < \mu_c$ the dipole dissociates beyond a maximum separation distance, namely the screening length L_s. We have also calculated the binding energy as a function of separation distance. In addition, we have presented $L_s(\eta)$ and found that there are qualitative consequences for quarkonium suppression in heavy ion collisions in this hQCD model.

We have calculated the free energy of the background black hole solution and further confirmed that there exists a first order phase transition in small μ region between small black hole and large black hole [15]. When $\mu > \mu_c$, the phase transition is absent from the point of view of the free energy. The existence of the critical point is consistent with the result in [15]. Further we have argued that there does not exist any phase transition

between black hole solutions and thermal gas solutions in this model, and the main reason is given.

In this work we have studied some aspects of QGP phase in the hQCD model proposed in [15]. The results are encouraged and are consistent with the expectation of real QCD. Thus it would be of great interest to further investigate the hQCD model. For example, it is required in the model to study the spectra of hadrons, chiral phase transition and its phase diagram [59][60][61], hydrodynamical properties of QGP, and color flavor locked phase [62][63][64], etc. Furthermore, quantum corrections [65] to above physical quantities are also deserved to consider in the coming works.

Finally we would like to mention that in this paper the drag force, jet quenching and screening length have been calculated through the Nambu-Goto action of fundamental string in the AdS/CFT correspondence. As one knows that the Nambu-Goto action makes sense only in string theory. Therefore it becomes a crucial issue whether our hQCD model can be embedded into some string theory. This is also a key point for a large kind of phenomenal models of holographic QCD. At the moment, we cannot show that the model could be a consistent truncation of some low energy effective theory of string theory, but we hope this model is helpful to build a holographic model dual to the realistic QCD.

Acknowledgements

The authors are grateful to Jiunn-Wei Chen, Xiaofang Chen, Danning Li, Sudipta Mukherji, Ajit M.Srivastava, Shi Pu, Wen-Yu Wen, Shang-Yu Wu, Chen-Pin Yeh, Yi Yang and Yun-Long Zhang for useful discussions. This work was supported in part by the National Natural Science Foundation of China (No.10821504, No.10975168 and No.11035008), and in part by the Ministry of Science and Technology of China under Grant No. 2010CB833004. SC wishes to thank the members of ITP, CAS for the warm hospitality during initial part of this work. SH would like to thank the Department of Electrophysics of National Chiao-Tung University, National Taiwan university and the "International School On Strings And Fundamental Physics" held at Hamburg, for their hospitality and financial support. SH also would like to appreciate the general financial support from China Postdoctoral Science Foundation with No. 2012M510562.

References

[1] K. Adcox *et al.* [PHENIX Collaboration], "Formation of dense partonic matter in relativistic nucleus-nucleus collisions at RHIC: Experimental evaluation by the PHENIX collaboration," Nucl. Phys. A **757**, 184 (2005) [nucl-ex/0410003].
J. Adams *et al.* [STAR Collaboration], "Experimental and theoretical challenges in the search for the quark gluon plasma: The STAR Collaboration's critical assessment of the evidence from RHIC collisions," Nucl. Phys. A **757**, 102 (2005) [nucl-ex/0501009].
B. B. Back, M. D. Baker, M. Ballintijn, D. S. Barton, B. Becker, R. R. Betts, A. A. Bickley and R. Bindel *et al.*, "The PHOBOS perspective on discoveries at RHIC," Nucl. Phys. A **757**, 28 (2005) [nucl-ex/0410022].

[2] E. Shuryak, "Physics of Strongly coupled Quark-Gluon Plasma," Prog. Part. Nucl. Phys. **62**, 48 (2009) [arXiv:0807.3033 [hep-ph]].

[3] E. V. Shuryak, "What RHIC experiments and theory tell us about properties of quark-gluon plasma?," Nucl. Phys. A **750**, 64 (2005) [hep-ph/0405066].

[4] R. Baier, Y. L. Dokshitzer, A. H. Mueller, S. Peigne and D. Schiff, "Radiative energy loss of high-energy quarks and gluons in a finite volume quark - gluon plasma," Nucl. Phys. B **483**, 291 (1997) [hep-ph/9607355]; K. J. Eskola, H. Honkanen, C. A. Salgado and U. A. Wiedemann, "The Fragility of high-p(T) hadron spectra as a hard probe," Nucl. Phys. A **747**, 511 (2005) [hep-ph/0406319].

[5] J. M. Maldacena, "The large N limit of superconformal field theories and supergravity," Adv. Theor. Math. Phys. **2**, 231 (1998) [Int. J. Theor. Phys. **38**, 1113 (1999)]; S. S. Gubser, I. R. Klebanov and A. M. Polyakov, "Gauge theory correlators from non-critical string theory," Phys. Lett. B **428**, 105 (1998); E. Witten, "The large N limit of superconformal field theories and supergravity," Adv.Theor.Math.Phys. 2 (1998) 253-291.

[6] O. Aharony, S. S. Gubser, J. M. Maldacena, H. Ooguri and Y. Oz, "Large N field theories, string theory and gravity," Phys. Rept. **323**, 183 (2000) [arXiv:hep-th/9905111].

[7] G. Policastro, D. T. Son and A. O. Starinets, "The shear viscosity of strongly coupled N = 4 supersymmetric Yang-Mills plasma," Phys. Rev. Lett. **87**, 081601 (2001) [arXiv:hep-th/0104066].

[8] P. Kovtun, D. T. Son and A. O. Starinets, "Holography and hydrodynamics: Diffusion on stretched horizons," JHEP **0310**, 064 (2003) [arXiv:hep-th/0309213].

[9] A. Buchel and J. T. Liu, "Universality of the shear viscosity in supergravity," Phys. Rev. Lett. **93**, 090602 (2004) [arXiv:hep-th/0311175].

[10] D. Teaney, "The Effects of viscosity on spectra, elliptic flow, and HBT radii," Phys. Rev. C **68**, 034913 (2003) [nucl-th/0301099].

[11] S. K. Chakrabarti, S. Chakrabortty and S. Jain, "Proof of universality of electrical conductivity at finite chemical potential," JHEP **1102**, 073 (2011) [arXiv:1011.3499 [hep-th]].

[12] S. He, M. Huang and Q. S. Yan, "Logarithmic correction in the deformed AdS_5 model to produce the heavy quark potential and QCD beta function," Phys. Rev. D **83**, 045034 (2011) [arXiv:1004.1880 [hep-ph]].

[13] D. Li, S. He, M. Huang and Q. S. Yan, "Thermodynamics of deformed AdS_5 model with a positive/negative quadratic correction in graviton-dilaton system," arXiv:1103.5389 [hep-th].

[14] S. He, Y. -P. Hu and J. -H. Zhang, "Hydrodynamics of a 5D Einstein-dilaton black hole solution and the corresponding BPS state," JHEP **1112**, 078 (2011) [arXiv:1111.1374 [hep-th]].

[15] R. -G. Cai, S. He and D. Li, "A hQCD model and its phase diagram in Einstein-Maxwell-Dilaton system," JHEP **1203**, 033 (2012) [arXiv:1201.0820 [hep-th]].

[16] S. He, M. Huang and Q. S. Yan, "Heavy quark potential and QCD beta function from a deformed AdS_5 model," Prog. Theor. Phys. Suppl. **186**, 504 (2010) [arXiv:1007.0088 [hep-ph]].

[17] C. P. Herzog, A. Karch, P. Kovtun, C. Kozcaz and L. G. Yaffe, "Energy loss of a heavy quark moving through N = 4 supersymmetric Yang-Mills plasma," JHEP **0607**, 013 (2006) [arXiv:hep-th/0605158].

[18] S. S. Gubser, "Drag force in AdS/CFT," Phys. Rev. D **74**, 126005 (2006) [arXiv:hep-th/0605182].

[19] P. B. Arnold, "Quark-Gluon Plasmas and Thermalization," Int. J. Mod. Phys. E **16** (2007) 2555 [arXiv:0708.0812 [hep-ph]].

[20] S. J. Sin and I. Zahed, "Ampere's law and energy loss in AdS/CFT duality," arXiv:hep-ph/0606049.

[21] C. P. Herzog, "Energy loss of heavy quarks from asymptotically AdS geometries," JHEP **0609**, 032 (2006) [arXiv:hep-th/0605191];

[22] J. J. Friess, S. S. Gubser and G. Michalogiorgakis, "Dissipation from a heavy quark moving through N = 4 super-Yang-Mills plasma," JHEP **0609**, 072 (2006) [arXiv:hep-th/0605292];

[23] J. Casalderrey-Solana and D. Teaney, "Heavy quark diffusion in strongly coupled N = 4 Yang Mills," Phys. Rev. D **74**, 085012 (2006) [arXiv:hep-ph/0605199].

[24] E. Caceres and A. Guijosa, "Drag force in charged N = 4 SYM plasma," JHEP **0611**, 077 (2006) arXiv:hep-th/0605235;

[25] S. Chakrabortty, "Dissipative force on an external quark in heavy quark cloud," Phys. Lett. B **705**, 244-255 (2011) [arXiv:1108.0165 [hep-ph]].

[26] J.D. Bjorken, *Energy Loss Of Energetic Partons In Quark - Gluon Plasma: Possible Extinction Of High P(T) Jets In Hadron - Hadron Collisions*, FERMILAB-PUB-82-059-THY

[27] S. S. Adler *et al.* [PHENIX Collaboration], "Nuclear modification of electron spectra and implications for heavy quark energy loss in Au+Au collisions at s(NN)**(1/2) - 200-GeV," Phys. Rev. Lett. **96**, 032301 (2006) [nucl-ex/0510047].

[28] J. Bielcik [STAR Collaboration], "Centrality dependence of heavy flavor production from single electron measurement in s(NN)**(1/2) = 200-GeV Au + Au collisions," Nucl. Phys. A **774**, 697 (2006) [nucl-ex/0511005].

[29] R. Baier, Y. L. Dokshitzer, A. H. Mueller, S. Peigne and D. Schiff, "Radiative energy loss and p(T)-broadening of high energy partons in nuclei," Nucl. Phys. B **484**, 265 (1997).

[30] F. D'Eramo, H. Liu and K. Rajagopal, "Transverse Momentum Broadening and the Jet Quenching Parameter, Redux," Phys. Rev. D **84**, 065015 (2011) [arXiv:1006.1367 [hep-ph]].

[31] A. Kovner and U. A. Wiedemann, "Gluon radiation and parton energy loss," In *Hwa, R.C. (ed.) et al.: Quark gluon plasma* 192-248 [hep-ph/0304151].

[32] A. Kovner and U. A. Wiedemann, "Eikonal evolution and gluon radiation," Phys. Rev. D **64**, 114002 (2001) [hep-ph/0106240].

[33] H. Liu, K. Rajagopal and U. A. Wiedemann, "Calculating the jet quenching parameter from AdS/CFT," Phys. Rev. Lett. **97**, 182301 (2006) [arXiv:hep-ph/0605178].

[34] E. Caceres and A. Guijosa, "On Drag Forces and Jet Quenching in Strongly Coupled Plasmas," JHEP **0612**, 068 (2006) [hep-th/0606134].

[35] A. Buchel, "On jet quenching parameters in strongly coupled non-conformal gauge theories," Phys. Rev. D **74**, 046006 (2006) [hep-th/0605178].

[36] J. F. Vazquez-Poritz, "Enhancing the jet quenching parameter from marginal deformations," hep-th/0605296.

[37] E. Nakano, S. Teraguchi and W. -Y. Wen, "Drag force, jet quenching, and AdS/QCD," Phys. Rev. D **75**, 085016 (2007) [hep-ph/0608274].

[38] S. D. Avramis and K. Sfetsos, "Supergravity and the jet quenching parameter in the presence of R-charge densities," JHEP **0701**, 065 (2007) [hep-th/0606190].

[39] Y. -h. Gao, W. -s. Xu and D. -f. Zeng, "Jet quenching parameters of Sakai-Sugimoto Model," hep-th/0611217.

[40] N. Armesto, J. D. Edelstein and J. Mas, "Jet quenching at finite 't Hooft coupling and chemical potential from AdS/CFT," JHEP **0609**, 039 (2006) [hep-ph/0606245].

[41] F. -L. Lin and T. Matsuo, "Jet Quenching Parameter in Medium with Chemical Potential from AdS/CFT," Phys. Lett. B **641**, 45 (2006) [hep-th/0606136].

[42] H. Liu, K. Rajagopal and U. A. Wiedemann, "An AdS/CFT Calculation of Screening in a Hot Wind," Phys. Rev. Lett. **98**, 182301 (2007) [hep-ph/0607062].

[43] E. Caceres, M. Natsuume and T. Okamura, "Screening length in plasma winds," JHEP **0610**, 011 (2006) [hep-th/0607233].

[44] M. Chernicoff, J. A. Garcia and A. Guijosa, "The Energy of a Moving Quark-Antiquark Pair in an N=4 SYM Plasma," JHEP **0609**, 068 (2006) [hep-th/0607089].

[45] M. Chernicoff and A. Guijosa, "Acceleration, Energy Loss and Screening in Strongly-Coupled Gauge Theories," JHEP **0806**, 005 (2008) [arXiv:0803.3070 [hep-th]].

[46] E. Kiritsis and V. Niarchos, "The holographic quantum effective potential at finite temperature and density," arXiv:1205.6205 [hep-th].

[47] S. W. Hawking and D. N. Page, "Thermodynamics of Black Holes in anti-De Sitter Space," Commun. Math. Phys. **87**, 577 (1983).

[48] E. Witten, "Anti-de Sitter space, thermal phase transition, and confinement in gauge theories," Adv. Theor. Math. Phys. **2**, 505 (1998) [arXiv:hep-th/9803131].

[49] C. P. Herzog, "A Holographic Prediction of the Deconfinement Temperature," Phys. Rev. Lett. **98**, 091601 (2007) [hep-th/0608151].

[50] R. -G. Cai and J. P. Shock, "Holographic confinement/deconfinement phase transitions of AdS/QCD in curved spaces," JHEP **0708**, 095 (2007) [arXiv:0705.3388 [hep-th]].

[51] U. Gursoy, E. Kiritsis, L. Mazzanti and F. Nitti, "Holography and Thermodynamics of 5D Dilaton-gravity," JHEP **0905**, 033 (2009) [arXiv:0812.0792 [hep-th]].

[52] A. Chamblin, R. Emparan, C. V. Johnson and R. C. Myers, "Charged AdS black holes and catastrophic holography," Phys. Rev. D **60**, 064018 (1999) [hep-th/9902170].

[53] A. Ficnar "AdS/CFT Energy Loss in Time-Dependent String Configurations" [arXiv:1201.1780 [hep-th]]

[54] J. Casalderrey-Solana, H. Liu, D. Mateos, K. Rajagopal and U. A. Wiedemann, "Gauge/String Duality, Hot QCD and Heavy Ion Collisions," arXiv:1101.0618 [hep-th].

[55] H. Liu, K. Rajagopal and U. A. Wiedemann, "Wilson loops in heavy ion collisions and their calculation in AdS/CFT," JHEP **0703**, 066 (2007) [arXiv:hep-ph/0612168].

[56] U. Gursoy, E. Kiritsis, G. Michalogiorgakis and F. Nitti, "Thermal Transport and Drag Force in Improved Holographic QCD," JHEP **0912**, 056 (2009) [arXiv:0906.1890 [hep-ph]].

[57] O. Kaczmarek and F. Zantow, "Static quark anti-quark interactions in zero and finite temperature QCD. I: Heavy quark free energies, running coupling and quarkonium binding," Phys. Rev. D71 (2005) 114510, [arXiv:hep-lat/0503017].

[58] M. Fromm, J. Langelage, S. Lottini and O. Philipsen, "The QCD deconfinement transition for heavy quarks and all baryon chemical potentials," JHEP **1201**, 042 (2012) [arXiv:1111.4953 [hep-lat]].

[59] N. Evans, A. Gebauer, K. -Y. Kim, "E, B, μ, T Phase Structure of the $D3/D7$ Holographic Dual," JHEP **1105**, 067 (2011). [arXiv:1103.5627 [hep-th]].

[60] N. Evans, K. -Y. Kim, J. P. Shock, J. P. Shock, "Chiral phase transitions and quantum critical points of the $D3/D7(D5)$ system with mutually perpendicular E and B fields at finite temperature and density," JHEP **1109**, 021 (2011). [arXiv:1107.5053 [hep-th]].

[61] N. Evans, A. Gebauer, K. -Y. Kim, "Towards a Holographic Model of the QCD Phase Diagram," [arXiv:1109.2633 [hep-th]].

[62] H. -Y. Chen, K. Hashimoto and S. Matsuura, "Towards a Holographic Model of Color-Flavor Locking Phase," JHEP **1002**, 104 (2010) [arXiv:0909.1296 [hep-th]].

[63] P. Basu, F. Nogueira, M. Rozali, J. B. Stang and M. Van Raamsdonk, "Towards A Holographic Model of Color Superconductivity," New J. Phys. **13**, 055001 (2011) [arXiv:1101.4042 [hep-th]].

[64] I. Shovkovy and M. Huang, "Gapless two flavor color superconductor," Phys. Lett. B **564**, 205 (2003) [hep-ph/0302142].

[65] A. Singh and A. Sinha, "Quantum corrections to screening at strong coupling," Nucl. Phys. B **864**, 167 (2012) [arXiv:1204.1817 [hep-th]].